Mixed-Valence Properties of an Acetate-Bridged Dinuclear Ruthenium (II,III) Complex

Reiner Lomoth,*,† Ann Magnuson,‡ Yunhua Xu,§ and Licheng Sun§

Department of Physical Chemistry, Uppsala University, P.O. Box 532, S-751 21 Uppsala, Sweden, Department of Biochemistry, Center for Chemistry and Chemical Engineering, Lund University, P.O. Box 124, S-221 00 Lund, Sweden, and Department of Organic Chemistry, Arrhenius Laboratories, Stockholm University, S-106 91 Stockholm, Sweden

Received: December 9, 2002; In Final Form: February 18, 2003

The mixed-valence dinuclear ruthenium complex $[Ru_2(bpmp)(\mu\text{-}OAc)_2]^{2+}$ (where bpmp is the phenolate anion of 2,6-bis[bis(2-pyridylmethyl) aminomethyl]-4-methylphenol, H-bpmp) has been studied by UV−Vis−NIR, IR, and EPR spectroscopic and electrochemical techniques. The $Ru_2^{II,III}$ complex undergoes reversible one-electron reduction ($E_{1/2} = -0.61$ V vs $Fc^{+/0}$) and oxidation ($E_{1/2} = 0.09$ V vs $Fc^{+/0}$), resulting in the $Ru_2^{II,II}$ and $Ru_2^{III,III}$ complexes, respectively. A comproportionation constant of $K_c = 1.10 \times 10^{12}$ ($\Delta G_c^\circ = -68$ kJ mol^{-1}) indicates considerable stability of the mixed-valence state. The paramagnetic complex displays a rhombic EPR spectrum ($g_1 = 2.492$; $g_2 = 2.242$; $g_3 = 1.855$) arising from a ground state in a $S = 1/2$ low spin system in a low symmetry environment. Three intense, distinguishable intervalence bands are observed in the NIR to mid-IR spectrum of $[Ru_2(bpmp)(\mu\text{-}OAc)_2]^{2+}$ at 3765 cm^{-1} ($\epsilon = 1840$ $M^{-1}cm^{-1}$), 5615 cm^{-1} ($\epsilon = 10590$ $M^{-1}cm^{-1}$), and 7735 cm^{-1} ($\epsilon = 3410$ $M^{-1}cm^{-1}$). All intervalence bands are symmetric but more narrow than predicted for the classical limit and independent of solvent polarity. The results of the spectroscopic and electrochemical characterization indicate that $[Ru_2(bpmp)(\mu\text{-}OAc)_2]^{2+}$ is either electronically delocalized (class III, $H_{ab} = 1880$ cm^{-1}) or at the borderline between localization and delocalization (class II−III, $H_{ab} \geq 590$ cm^{-1}) with rapid electron transfer ($k_{ET} > 4 \times 10^{12}$ s^{-1}) decoupled from solvent reorientation but with a residual activation barrier ($E_a \leq 440$ cm^{-1}) from inner reorganization.

Introduction

Mixed-valence compounds have potential applications as, for example, superconductors[1] and materials for molecular electronics[2] and nonlinear optics.[3] Systems with strong electronic coupling at the borderline between localization and delocalization have attracted particular interest owing to the rapid electron transfer in these compounds.[4]

The effects of delocalization on the electronic spectra have been studied extensively in the past decades[5] and were reasonably well explained by the semiclassical models of Hush[6] and Sutin[7] and have also been treated quantum mechanically.[8] Narrow and solvent-independent intervalence bands are associated with delocalization, i.e., strong coupling and no net charge transfer in the intervalence transition (class III in the classification scheme of Robin and Day[9]). However, Meyer and coworkers have pointed out that these experimental criteria can be misleading if intramolecular electron transfer in a localized compound (class II) is fast compared to reorganization of the solvent dipoles.[10] In that case, coupling of electron transfer to the solvent is lost and intervalence bands become narrow and solvent independent, properties usually attributed to delocalized compounds in class III. The combination of electronic localization and solvent averaging has been reported for pyrazine- and N_2-bridged osmium complexes and defines another class of mixed-valence compounds referred to as class II−III.[10]

Here we report the mixed-valence properties of a novel diruthenium complex $[Ru_2(bpmp)(\mu\text{-}OAc)_2]^{2+}$ with a phenoxo and two acetato bridges where H-bpmp is the binucleating ligand 2,6-bis[bis(2-pyridylmethyl)aminomethyl]-4-methylphenol.[11] The complex that features a nonlinear bridging structure and a short metal-to-metal distance exhibits three distinguishable intervalence bands.[12] We report and discuss the electrochemical and spectroscopic properties of $[Ru_2(bpmp)(\mu\text{-}OAc)_2]^{2+}$ in view of electronic delocalization. Our results indicate that the mixed-valence complex is either delocalized (class III) or at the borderline between localization and delocalization (class II−III).

SCHEME 1

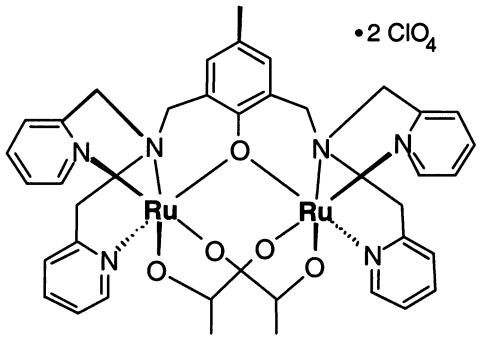

Methods and Materials

Materials. *$[Ru_2(bpmp)(\mu\text{-}OAc)_2](ClO_4)_2$.* H-bpmp was prepared following a procedure described elsewhere.[13] NaOAc (181 mg, 2.15 mmol) and $Ru(DMSO)_4Cl_2$ (247 mg, 0.51 mmol) were added to a degassed solution of H-bpmp (108 mg, 0.204 mmol) in 7 mL methanol. The yellow solution was degassed for another

* Corresponding author. E-mail: reiner.lomoth@fki.uu.se
† Uppsala University.
‡ Lund University.
§ Stockholm University.

10.1021/jp022563y CCC: $25.00
Published on Web 05/10/2003

5 min. The mixture was refluxed for 3 h, during which the color of the reaction mixture changed from yellow to brownish red, and was then allowed to cool to room temperature. $NaClO_4 \cdot H_2O$ (700 mg, 5 mmol) dissolved in 1 mL of H_2O was added to the reaction mixture, and a brownish-red precipitate appeared. The precipitate was filtered and washed with H_2O and ether and dried in a vacuum to afford the desired ruthenium complex (190 mg, 89%yield). In the course of the complexation reaction, oxidation of the ruthenium(II,II) complex by air occurred resulting in the mixed-valence ruthenium(II,III) complex. ESI-MS: 950.1 (calcd for $[M\text{-}ClO_4^-]^+$, 950.1) and 425.6 (calcd for $[M\text{-}2ClO_4^-]^{2+}$, 425.6); elemental analysis (%) calcd for $C_{37}H_{39}Cl_2N_6O_{13}Ru_2$: C 42.37, H 3.75, N 8.01; found: C 42.07, H 3.79, N 7.87.

Electrochemistry. Cyclic voltammetry, differential pulse voltammetry, and controlled potential electrolysis were performed with an Autolab potentiostat (Eco Chemie) connected to a standard three-electrode cell. The working electrode was a glassy carbon disk (diameter 3 mm) for voltammetry or a Pt-grid cylinder for coulometry. A platinum spiral in a compartment separated from the bulk solution by a fritted disk was used as counter electrode. The reference electrode was a nonaqueous $Ag^{+/0}$ electrode (CH Instruments, 10 mM $AgNO_3$ in acetonitrile) connected to the solution via a salt bridge (0.1 M $TBAClO_4$). The reference electrode had a potential of −0.08 V vs. the ferocenium/ferrocene ($Fc^{+/0}$) couple in acetonitrile as an external standard. All potentials reported here are vs. $Fc^{+/0}$ and have been converted by adding −0.08 V to the potentials measured vs. the $Ag^{+/0}$ electrode.

Electrolyte solution was prepared from dry acetonitrile (Merck, spectroscopy grade, dried with MS 3 Å) with 0.1 M tetrabutylammonium perchlorate ($TBAClO_4$, Fluka, electrochemical grade, dried at 373 K) as supporting electrolyte. Before all measurements, solutions were deoxygenated by bubbling the stirred solutions for 10 min with solvent-saturated argon and while measuring the samples were kept under argon atmosphere.

UV−Vis−NIR Spectroscopy: Spectra between 200 and 2700 nm were recorded on a Varian spectrophotometer (CARY 2400).

UV−Vis spectroelectrochemical measurements between 200 and 2700 nm were made in an OTTLE-type quartz cell with an optical path length of 1 mm. A platinum grid with a size of 10 × 30 mm^2 and 400 meshes per cm^2 was used as working electrode. The counter and reference electrodes are of the same type as described in the electrochemistry paragraph.

The samples were bubbled for 20 min with solvent saturated argon and transferred to the argon-flushed cell with the argon stream. Spectra were recorded on an UV−Vis diode array spectrophotometer (Hewlett-Packard 8435) and an UV−Vis−NIR spectrophotometer (Varian CARY 2400).

IR Spectroscopy. IR spectra between 400 and 5000 cm^{-1} were recorded on a Bruker FT-IR spectrometer (IFS 66v/S) with the sample as a KBr pellet or as solution between KBr windows.

IR spectroelectrochemical measurements between 500 and 5000 cm^{-1} were performed in transmission mode in a thin layer cell equipped with ZnSe windows and the optical path length set to 120 μm. The working electrode was a Pt grid (1024 meshes per cm^2, 65% open area), the counter electrode was a Pt cylinder concentric with the working electrode, and the reference electrode was of the same type as described for electrochemistry and connected to the cell via a salt bridge (0.5 M $LiClO_4$ in CH_3CN).

Electrolyte solution for IR spectroelectrochemistry was prepared from CD_3CN− (Aldrich, 99.8 atom-% D) with 0.5 M $LiClO_4$ (Aldrich) as supporting electrolyte.

EPR Spectroscopy. EPR measurements were performed on a Bruker E500 X-band spectrometer equipped with a Bruker dual-mode cavity and an Oxford Instruments temperature controller and ESR900 flow cryostat. All spectra were recorded at cryogenic temperatures (5−20 K, see figure legends for details), the modulation amplitude in all measurements was 10 G, the modulation frequency was 100 kHz, and the microwave frequency was 9.62 GHz.

With a delocalization parameter $\alpha^2 = (H_{ab}/E_{IV})^2 = 0.025$[14] in the ground state the mixed-valence dimer was considered as localized,[15] i.e., the Ru^{III} center of the complex was treated like a monomeric low-spin Ru^{III} complex and the zero field splitting parameters and energies of the IC excited states were calculated following published procedures.[16] The proper assignment of the observed g values g_n ($n = 1, 2, 3$) to the principal g values g_i ($i = x, y, z$) and the choice of the signs were made in a way that fulfilled the following criteria: (i) normalization of the resulting coefficients $A_1^2 + B_1^2 + C_1^2 = 0$; (ii) $|V/\Delta| \leq 2/3$; and (iii) $V \geq 0$. With the assignment of $g_x = 2.4919$, $g_y = 2.2418$, and $g_z = 1.8549$, a normalization of $A_1^2 + B_1^2 + C_1^2 = 0.998$ was obtained. A, B, and C are coefficients describing the Kramers doublets $|\Psi_i^{\pm}\rangle$ ($i = 1, 2, 3$) as linear combinations

$$|\Psi_i^{+}\rangle = A_i|+1, +1/2\rangle + B_i|0, -1/2\rangle + C_i|-1, +1/2\rangle$$

$$|\Psi_i^{-}\rangle = A_i|-1, -1/2\rangle - B_i|0, +1/2\rangle + C_i|+1, -1/2\rangle$$

of the basis functions $|M_L, M_S\rangle$ that form the 3-fold orbitally degenerate $^2T_{2g}$ ground state with $L = 1$ and $S = 1/2$ for a low-spin Ru^{III} configuration.

Results and Discussion

Electrochemistry. A cyclic voltammogram of $[Ru_2(bpmp)(\mu\text{-}OAc)_2]^{2+}$ in acetonitrile is shown in Figure 1. Reversible one-electron reduction and oxidation occurs at $E_{1/2} = -0.61$ V vs $Fc^{+/0}$ and $E_{1/2} = 0.09$ V vs $Fc^{+/0}$, respectively. Reversibility of the reduction and oxidation reaction is confirmed by peak splits of $\Delta E_p = 60-70$ mV and the ratio of anodic to cathodic peak currents $i_{pa}/i_{pc} = 1$. The one-electron nature of these reactions has been confirmed by coulometry during controlled potential electrolysis at −0.88 and 0.32 V vs $Fc^{+/0}$. The voltammograms of a solution after exhaustive reduction (−0.88 V), reoxidation (−0.33 V), oxidation (0.32 V), and rereduction (−0.33 V) are identical with the initial voltammogram excluding degradation reactions of the ruthenium complex in the isovalent forms. The reversible one-electron reduction and oxidation are assigned to the metal centered reactions 1 and 2.

$$[Ru_2^{II,III}(bpmp)(\mu\text{-}OAc)_2]^{2+} + e^- \rightleftarrows [Ru_2^{II,II}(bpmp)(\mu\text{-}OAc)_2]^{+} \quad E_{1/2} = -0.61 \text{ V} \quad (1)$$

$$[Ru_2^{II,III}(bpmp)(\mu\text{-}OAc)_2]^{2+} \rightleftarrows [Ru_2^{III,III}(bpmp)(\mu\text{-}OAc)_2]^{3+} + e^- \quad E_{1/2} = 0.09 \text{ V} \quad (2)$$

From the separation $\Delta E_{1/2} = 0.70$ V of the half-wave potentials a comproportionation constant $K_c = \exp(\Delta E_{1/2}\, F/RT) = 1.10 \times 10^{12}$ (at 293 K) can be calculated reflecting the pronounced stability of the mixed-valence state. However, K_c cannot provide a direct measure of delocalization since it is affected not only by resonance exchange but also by electrostatic, statistic, and synergistic effects. Assuming localization resonance exchange (as inferred from spectroscopic measurements, see below) contributes only $\Delta G^\circ_{ex} = -0.011$ eV, i.e., 3.2%, to the standard

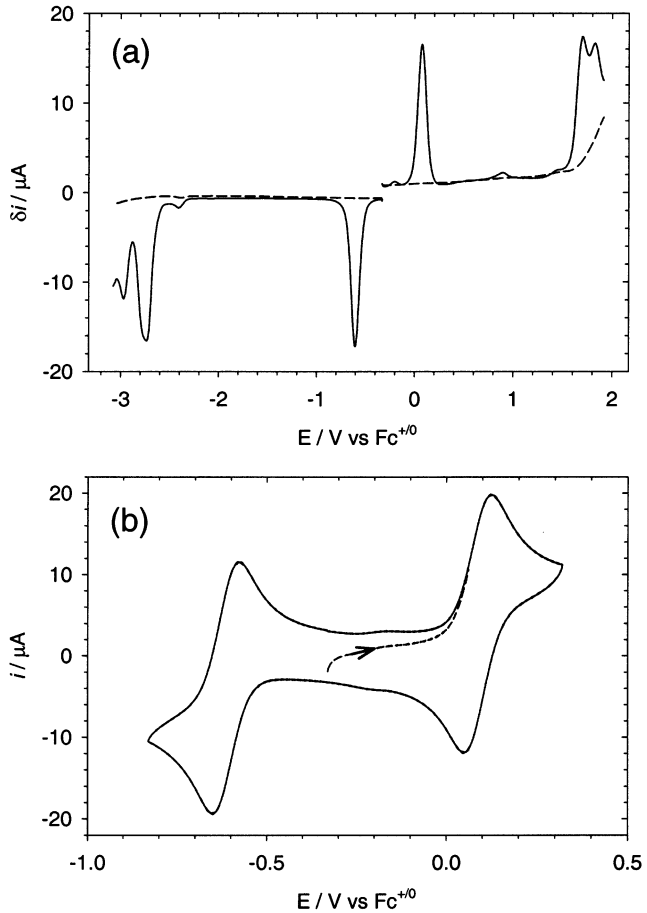

Figure 1. Voltammograms of $[Ru_2(bpmp)(\mu\text{-}OAc)_2]^{2+}$ (1 μM) in CH_3CN with 0.1 M $[(n\text{-}C_4H_9)_4N][PF_6]$ as supporting electrolyte. (a) Differential pulse voltammogram. Dashed line: electrolyte background. (b) Cyclic voltammogram ($v = 0.100$ V s^{-1}).

free energy of comproportionation, then $\Delta G°_c/2 = -0.35$ eV (per $[Ru_2(bpmp)(\mu\text{-}OAc)_2]^{2+}$). In the delocalized case $\Delta H°_{ex} = 0.233$ eV would account for 67% of $\Delta G°_c/2$. A substantial contribution to $\Delta G°_c$very likely arises from Coulombic effects due to the relatively short metal−metal distance. Under this circumstance the magnitude of $K_c = 1.10 \times 10^{12}$ does not provide evidence for delocalization. This is demonstrated by the Fe analogue $[Fe_2(bpmp)(\mu\text{-}O_2C{-}C_2H_5)_2]^{2+}$ with $K_c = 1.63 \times 10^{12}$ that is localized as evidenced by crystallographic and Mössbauer data.[17]

Additional reductions and oxidations of $[Ru_2(bpmp)(\mu\text{-}OAc)_2]^{2+}$ occur at more extreme potentials (see DPV, Figure 1 a). Reduction at $E_{pk} = -2.73$ V (DPV peak potential) can be assigned to a ligand-based reduction by comparison to voltammograms of the ligand (not shown). Further oxidations occur at the limit of the solvent window ($E_{pk} = 1.67$ V, $E_{pk} = 1.82$ V) impeding spectroelectrochemical and coulometric experiments. The voltammetric peak height suggests that the oxidation at 1.67 V is a one-electron process that might be tentatively assigned to the $Ru_2^{III,IV}/Ru_2^{III,III}$ couple.

EPR Spectroscopy. When $[Ru_2(bpmp)(\mu\text{-}OAc)_2]^{2+}$ was investigated by EPR at 15 K, a broad EPR spectrum of approximately 1200 G was observed, displaying large rhombic *g* anisotropy (Figure 2 a), which is in agreement with a mixed valence complex in the $Ru_2^{II,III}$ state. The temperature dependence of the signal amplitude (not shown) indicated that the signal arises from a ground state, in an S = 1/2 low spin system. The three *g* values are $g_1 = 2.492$; $g_2 = 2.242$, and $g_3 = 1.855$, respectively. The large deviation from the free electron *g*-value

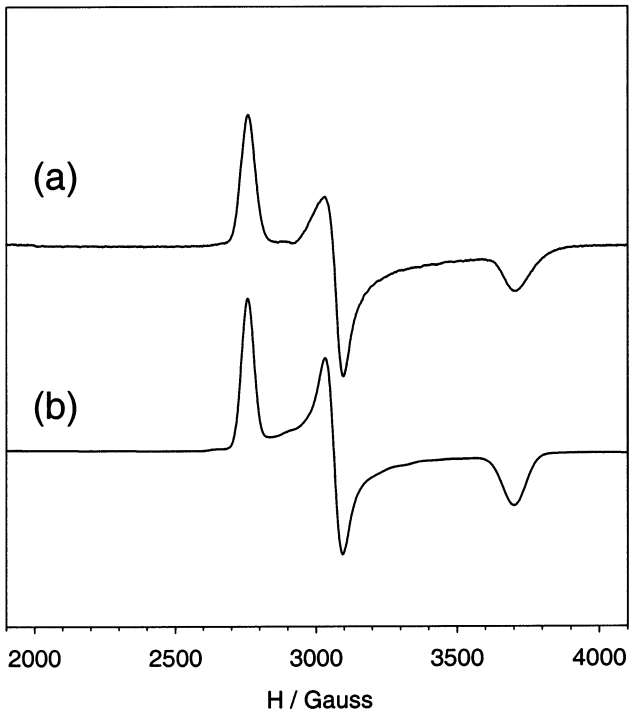

Figure 2. (a) EPR spectrum of $[Ru_2(bpmp)(\mu\text{-}OAc)_2]^{2+}$ in frozen acetonitrile solution. $T = 15$ K; Microwave power = 0.2 mW. (b) Simulated spectrum using a localized Ru^{III} model. The *g* values are $g_1 = 2.492$; $g_2 = 2.242$; and $g_3 = 1.855$.

is typical for metal complexes with a large spin−orbit coupling, as in the case of ruthenium. Similar EPR spectra have been observed earlier in several other $Ru_2^{II,III}$ complexes, where the large *g* anisotropy is caused by a low symmetry environment of the Ru^{III} ion.[18] For symmetry reasons (no symmetry axis of order >2), a rhombic **g** tensor is expected for $[Ru_2(bpmp)(\mu\text{-}OAc)_2]^{2+}$, irrespective of the degree of delocalization. The spectrum could be accurately simulated assuming a localized S = 1/2 system, i.e., treating the system as an isolated Ru^{III} ion (Figure 2b). However, the absence of any detectable ^{99,101}Ru hyperfine coupling did not allow us to infer the degree of delocalization from the EPR spectrum.[19]

From the *g* matrix, the zfs parameters Δ and *V* and the energies ϵ_1 and ϵ_2 between ground state and excited states were calculated assuming complete localization of the ground state and neglecting covalency and configuration interaction by taking the orbital reduction factor as unity. Within this approximation $\Delta/\zeta = -5.37$ and $V/\zeta = 2.81$ were obtained, where $\zeta \approx 1000$ cm^{-1} is the one-electron spin−orbit coupling constant for Ru^{3+}. The excited-state energies $\epsilon_1/\zeta = 4.10$ and $\epsilon_2/\zeta = 7.05$ substantially exceed the values estimated from the electronic spectrum (see NIR spectroscopy), indicating that the approximations made in the analysis of the *g* matrix do not apply for $[Ru_2(bpmp)(\mu\text{-}OAc)_2]^{2+}$.

UV−Vis Spectroscopy. Figure 3a shows the UV−vis spectrum of $[Ru_2(bpmp)(\mu\text{-}OAc)_2]^{2+}$ recorded in acetonitrile. Spectra of $[Ru_2(bpmp)(\mu\text{-}OAc)_2]^{+}$ and $[Ru_2(bpmp)(\mu\text{-}OAc)_2]^{3+}$ have been observed by spectroelectrochemistry. Several sharp isosbestic points have been kept in the course of the reduction (233, 246, 255, 368, and 665 nm) and oxidation (236, 256, 318, 505, and 800 nm). Complete recovery of the initial spectrum of $[Ru_2(bpmp)(\mu\text{-}OAc)_2]^{2+}$ has been observed upon reoxidation (−0.38 V) and rereduction (−0.13 V), providing further evidence as to the chemical reversibility of the oxidation and reduction reactions.

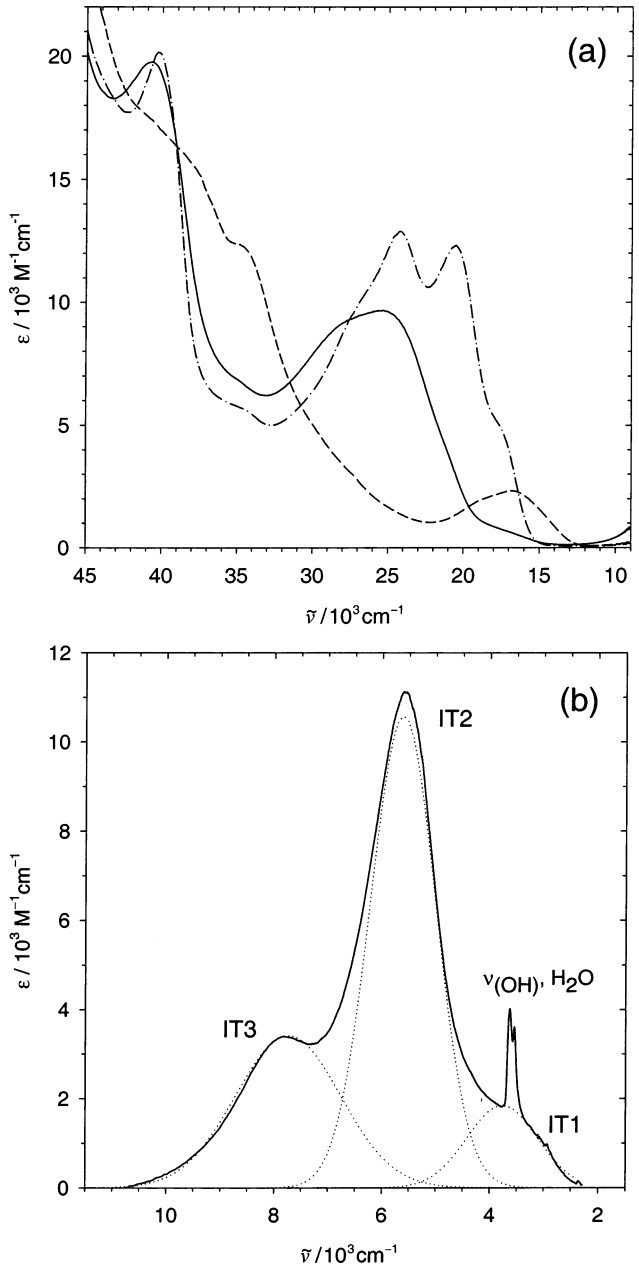

Figure 3. Absorption spectra of $[Ru_2(bpmp)(\mu\text{-}OAc)_2]^{2+}$ (—), $[Ru_2(bpmp)(\mu\text{-}OAc)_2]^{3+}$ (- - -), and $[Ru_2(bpmp)(\mu\text{-}OAc)_2]^{+}$ (-•-) in the UV−Vis (a) and NIR to mid-IR range (b). Gaussian peaks (•••) fitted to the spectrum of $[Ru_2(bpmp)(\mu\text{-}OAc)_2]^{2+}$ omitting $\nu_{(OH)}$. All spectra in CH_3CN. Spectra of $[Ru_2(bpmp)(\mu\text{-}OAc)_2]^{3+}$ and $[Ru_2(bpmp)(\mu\text{-}OAc)_2]^{+}$ were obtained spectroelectrochemically by electrolysis at 0.32 V and −0.88 V.

By comparison to the spectrum of the ligand (not shown), the intense UV absorption above 38000 cm^{-1} can be assigned to the ligand-based $\pi-\pi^*$ transitions of the aromatic ligand functions and accordingly is only slightly affected by the oxidation states of the metal centers.

The strong visible absorption of the reduced complex $[Ru_2(bpmp)(\mu\text{-}OAc)_2]^{+}$ (Figure 3a, -•-) with peaks at 24400 cm^{-1} (410 nm, $\epsilon = 12.9 \times 10^4$ M^{-1} cm^{-1}) and 20410 cm^{-1} (490 nm, $\epsilon = 12.3 \times 10^4$ M^{-1} cm^{-1}) together with shoulders at 27000 cm^{-1} and 17500 cm^{-1} can be assigned to MLCT transitions from the t_2 orbitals of Ru^{II} to ligand orbitals. Multiple CT transitions can result from the splitting of the metal orbitals due to the reduced symmetry or from the presence of several acceptor orbitals in the mixed-ligand complex.

SCHEME 2

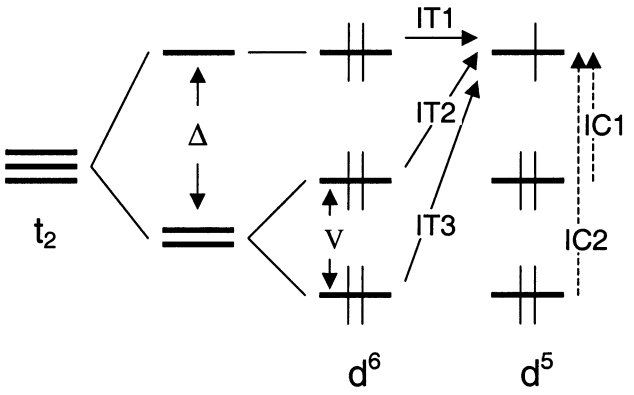

The spectrum of the oxidized complex $[Ru_2(bpmp)(\mu\text{-}OAc)_2]^{3+}$ (Figure 3a, - - -) lacks the intense bands in the blue part of the spectrum of the $Ru_2^{II,II}$ complex and instead displays a much weaker band with maximum at 16670 cm^{-1} (600 nm, $\epsilon = 2.3 \times 10^3$ M^{-1} cm^{-1}) that can be assigned to a LMCT transition from a ligand orbital to Ru^{III}.

In the mixed-valence state the spectra in the UV−vis range (Figure 3a, −) cannot be described as the average of the isovalent $Ru_2^{II,II}$ and $Ru_2^{III,III}$ complexes, indicating substantial interaction between the metal sites.

NIR Spectroscopy. In the near- to mid-IR range (Figure 3b) the mixed valence complex shows three intense absorption bands, of which the lowest energy band overlaps with parts of the vibrational spectrum. Spectroelectrochemical measurements (−0.88 and 0.32 V) have shown that the bands labeled as IT 1, IT 2, and IT 3 are not observed, with the isovalent forms of the complex providing strong evidence of the assignment of these bands to intervalence charge-transfer transitions.

They can be attributed to transitions from the t_2 orbitals of the Ru^{II} center (d^6) to the singly occupied t_2 orbital of the Ru^{III} center (d^5). The degeneracy of the t_2 orbitals is lifted by axial (Δ) and rhombic (V) distortion and spin−orbit coupling, giving rise to the energy differences between the IT bands as schematically depicted in Scheme 2.

For first and second row transition metal complexes, multiple IT bands are usually not sufficiently separated and the fact that distinguishable IT bands could be observed with $[Ru_2(bpmp)(\mu\text{-}OAc)_2]^{2+}$ points to a largely asymmetric ligand field in agreement with the EPR spectrum. The interconfigurational (IC) transitions between the splitted t_2 orbitals of the Ru^{III} centers were not observed with $[Ru_2^{II,III}(bpmp)(\mu\text{-}OAc)_2]^{2+}$. They could in principle serve as oxidation state markers indicative for Ru^{III}, but the parity forbidden transitions were not detectable in the isovalent $Ru_2^{III,III}$ state and, therefore, the absence of this bands in the spectrum of $Ru_2^{II,III}(bpmp)(\mu\text{-}OAc)_2]^{2+}$ is not in conflict with a localized description of the mixed-valence state.

The spectrum can be reasonably fitted by three Gaussian bands (dotted lines Figure 3b) if the strong vibrational band (ν_{O-H}, water) is omitted. Energies E_{IT}, half-widths $\Delta\tilde{\nu}_{1/2}$, and extinction coefficients ϵ obtained from this fit are given in Table 1.

All IT bands are more narrow than predicted by eq 3 (see Table 1) for the limit of $2H_{ab}/\lambda \ll 1$, indicating substantial coupling.

$$(\Delta\tilde{\nu}_{1/2})^2 = 16k_BT\lambda \ln 2 = 2.31 \times 10^3(E_{IT} - \Delta G^\circ) \quad \text{(at 298 K in cm}^{-1}\text{)} \quad (3)$$

TABLE 1: Analysis of the Intervalence Bands for $[Ru_2(bpmp)(\mu\text{-}OAc)_2]^{2+}$

	E_{IT}/ cm^{-1}	$\Delta\tilde{\nu}_{1/2}$/ cm^{-1}	ϵ/ $M^{-1}\,cm^{-1}$	λ/ cm^{-1}	H_{ab}[a]/ cm^{-1}	$2H_{ab}/\lambda$	E_a/ cm^{-1}
IT1	3765	1300 (2950)[b]	1840	3765	590	0.31	440
IT2	5615	1215 (3600)[b]	10590	3765[c]	1660	0.88	10
IT3	7735	1950 (4230)[b]	3410	3765[c]	1410	0.75	60

[a] Calculated with eq 4 and $d = 3.3$ Å. [b] Calculated with eq 3. [c] Equal λ in ground and excited states assumed.

Narrowing at the low energy side is predicted if $2H_{ab}/\lambda > (1 - \Delta\tilde{\nu}_{1/2}/2\lambda)$ resulting in asymmetric IT bands (class IIB) and a complete cutoff at $\tilde{\nu} = 2H_{ab}$ if $2H_{ab}/\lambda \geq 1$ (class III).[20] With a three-state model, Sutin et al. have shown that this prediction is also valid for bridge-mediated intervalence transfer.[21] Thus, the symmetric shape of the IT bands points to localization while they are unusually narrow for a localized complex. Meyer and co-workers have reported unusually narrow IT bands for electronically localized Os dimers and have attributed this to the decoupling of the solvent from the fast electron transfer that would also explain low energies of the IT bands and the absence of a solvent effect (see below).[10]

The energy of the IT bands is $E_{IT} = \Delta G^\circ + \lambda$ with the free energy change ΔG° and the reorganization energy λ of the intramolecular charge-transfer reaction, regardless of the degree of localization as long as the system is valence trapped. By contrast $E_{IT} = 2H_{ab}$ if the complex comes under class III.

In a localized, symmetric complex, no free energy change ΔG° occurs for the IT charge-transfer reaction in the ground state and $E_{IT}(1)$ is equal to λ. It is usually assumed that the reorganization energies for IT charge transfer are identical in the ground and the excited states. With this assumption, $E_{IT}(2) \approx \epsilon_1 + \lambda$ and $E_{IT}(3) \approx \epsilon_2 + \lambda$ result in estimates of $\epsilon_1 \approx 1800$ cm^{-1} and $\epsilon_2 \approx 4000$ cm^{-1}. From the energy-coordinate diagram (Figure 4) simillar values of ϵ_1 and ϵ_2 between the diabatic states are obtained when the adiabatic curves are displaced to match the observed energies of IT 2 and IT 3. Values of ϵ_1 and ϵ_2 cannot be inferred directly from the electronic spectrum since the corresponding IC transitions were not observed (see above).

The electronic coupling matrix elements H_{ab} have been calculated from the parameters of the IT bands with the equation derived by Hush (eq 4).

$$H_{ab}(cm^{-1}) = [(4.2 \times 10^{-4})\epsilon\Delta\tilde{\nu}_{1/2}E_{IT}]^{1/2}/d \qquad (4)$$

The electron-transfer distance d can be shorter than the geometrical center-to-center distance as a result of orbital mixing with bridge-based orbitals or orbitals of the redox sites. The effective electron-transfer distance is difficult to determine, and the values in Table 1 have been calculated with $d = 3.3$ Å as an upper limit.[22] This value is typically found for the geometric center-to-center distance in Ru_2 complexes with a $(\mu\text{-O})(\mu\text{-R}-COO)_2$ or $(\mu\text{-OH})(\mu\text{-R}-COO)_2$ core.[23]

Valence delocalization occurs if $2H_{ab}/\lambda \geq 1$ and the value of $2H_{ab}/\lambda = 0.31$ obtained from Hush analysis implies that the ground state of the complex is electronically localized. In the IC excited states, however, $2H_{ab}/\lambda$ is closer to unity and the electronic structure is close to delocalized with activation barriers much smaller than k_BT (Table 1). The activation barrier to intramolecular electron transfer E_a was calculated using eq 5.

$$E_a = \frac{\lambda}{4} - |H_{ab}| + \frac{H_{ab}^{\,2}}{\lambda} \qquad (5)$$

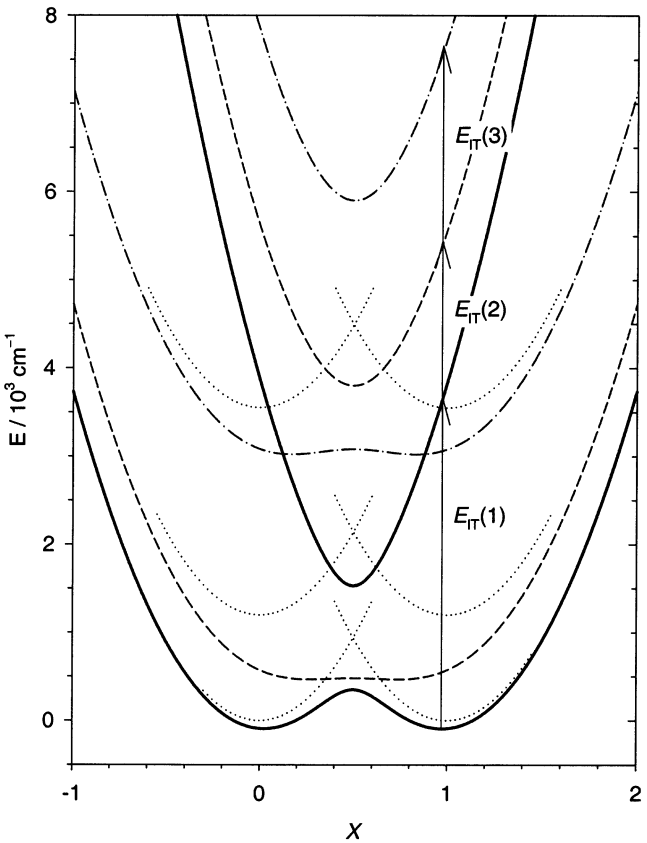

Figure 4. Energy-coordinate diagrams for the ground state (—) and the first (- - -) and second (-•-) interconfigurational (IC) excited states of $[Ru_2(bpmp)(\mu\text{-}OAc)_2]^{2+}$ plotted with the values from Table 1. The minimum of the diabatic ground state is defined as zero energy. The adiabatic curves of the excited states were displaced vertically according to the observed energies of IT 2 and IT 3. Arrows indicate intervalence transitions. The energies $E_\pm = (1/2)[\lambda(2X^2 - 2X + 1)] \pm (1/2)\{[\lambda(2X - 1)]^2 + 4H_{ab}^2\}^{1/2}$ of the lower and upper adiabatic states are described as a function of the reduced coordinate $X = x/a$ where x describes an average of coupled nuclear motions assumed to be harmonic with equal force constants f for reactants and products. The displacement between the energy minima of reactants and products is a and $\lambda = fa^2/2$.

Figure 4 shows energy-coordinate diagrams of the ground state and the IC excited states plotted with the parameters from Table 1. The stabilization of the ground state relative to the diabatic states (dotted lines) inferred from the spectroscopic measurements is $\Delta G^\circ_{ex} = H_{ab}^2/\lambda = -92$ cm^{-1} in the localized case, i.e., a minor fraction of the overall stabilization $\Delta G^\circ_c/2 = -2823$ cm^{-1} (per $[Ru_2(bpmp)(\mu\text{-}OAc)_2]^{2+}$). By contrast $\Delta H^\circ_{ex} = H_{ab} = 1883$ cm^{-1} would account for a major fraction of $\Delta G^\circ_c/2$ if $[Ru_2(bpmp)(\mu\text{-}OAc)_2]^{2+}$ was delocalized (see electrochemistry).

With the parameters of the Hush analysis, the energy-coordinate diagram for the ground state shows pronounced minima for the product and reactant states and an activation barrier $E_a = 440$ cm^{-1} to electron transfer between the metal sites. This should result in a sizable net charge transfer and make the energy of the related IT band strongly solvent dependent owing to the contribution of the outer reorganization energy.

However, no solvent effect on the IT bands was observed. All data obtained from the NIR spectrum of $[Ru_2(bpmp)(\mu\text{-}OAc)_2]^{2+}$ compiled in Table 1 was obtained in acetonitrile solution ($1/n - 1/\epsilon = 0.526$), but IT bands identical in energy, intensity, and shape were observed in the following solvents: methanol (0.534), dichloromethane (0.481), formamide (0.467), and dimethyl sulfoxide (0.435).

Narrow, solvent-independent IT bands are usually considered as evidence of valence delocalization, putting the complex in class III where the IT bands arise from transitions between delocalized electronic levels rather than from charge transfer. As pointed out by Meyer and co-workers, solvent independent IT bands at low energies can also be a result of solvent averaging and cannot serve as a proper criterion for valence delocalization.[10] In case of localization, the solvent-independent IT bands of $[Ru_2(bpmp)(\mu\text{-}OAc)_2]^{2+}$ would require that electron transfer is rapid on the time scale of solvent reorientation. If these motions cannot contribute to the electron-transfer barrier ($\lambda_o = 0$) the residual barrier arises only from intramolecular structural changes, making the IT bands solvent-independent ($E_{IT} = \lambda_i$) and explaining the low energies and narrow bandwidths of the IT bands.

In this case $[Ru_2(bpmp)(\mu\text{-}OAc)_2]^{2+}$ would be electronically localized but with an averaged orientation of the surrounding solvent dipoles. The average relaxation time for CH_3CN is about 260 fs,[24] putting a lower limit of $k_{ET} = 4 \times 10^{12}$ s^{-1} on the electron-transfer rate constant.

With the values of H_{ab} and λ given in Table 1, an electron tunneling frequency of $\nu_{el} = 1.3 \times 10^{14}$ s^{-1} can be calculated with eq 6.[25]

$$\nu_{el} = \frac{4\pi^2 H_{ab}^2}{h}\left(\frac{1}{4\pi\lambda k_B T}\right)^{1/2} \quad (6)$$

Hence, electron transfer will occur in the adiabatic regime where the barrier crossing frequency is dictated by the nuclear vibration frequency, and an electron-transfer rate constant $k_{ET} = \nu_n \exp(-E_a/k_B T)$ sufficiently fast to result in solvent averaging requires $\nu_n \geq 4 \times 10^{13}$ s^{-1} (at 298 K). Thus, electron transfer has to be coupled to vibrational modes of relatively high frequency ($\tilde{\nu} \geq 1300$ cm^{-1}). This appears to be consistent with the IR spectrum (see below) that suggests coupling of the asymmetric acetate stretch vibration (1473 cm^{-1} in the mixed-valence state) to electron transfer in $[Ru_2(bpmp)(\mu\text{-}OAc)_2]^{2+}$.

IR Spectroscopy. The mid-IR spectrum of $[Ru_2(bpmp)(\mu\text{-}OAc)_2]^{2+}$ was recorded in the solid state (as KBr disk) and in acetonitrile-d_3 solution. The mid-IR spectra of the isovalent forms of the complex were obtained spectroelectrochemically.

On the basis of characteristic frequencies, the assignment of the following bands is straightforward: 3004 cm^{-1} (vw, $\nu_{(C-H)}$, aryl), 2944 cm^{-1} (w, $\nu_{(C-H)}$, alkyl), 1102 cm^{-1} (vs, $\nu_{a(Cl-O)}$, ClO_4^-), 625 cm^{-1} (m, $\delta_{a(Cl-O)}$, ClO_4^-). Water in the preparation of $[Ru_2(bpmp)(\mu\text{-}OAc)_2]^{2+}$ gave rise to bands at 3360, 3546 cm^{-1} ($\nu_{(O-H)}$), and 1633 cm^{-1} ($\delta_{(H-O-H)}$).

Figure 5 shows the part of the IR spectra of $[Ru_2(bpmp)(\mu\text{-}OAc)_2]^{2+}$ and its isovalent states in acetonitrile-d_3 solution where bands arise from the acetate and pyridyl ligands. The asymmetric and symmetric stretching modes, $\nu_{a(COO)}$ and $\nu_{s(COO)}$, of bridging acetate ligands generally occur in the 1500−1600 cm^{-1} and 1400−1450 cm^{-1} range, respectively.[26] In the same range, bands of the H-bpmp ligand are observed at, e.g., 1430, 1475, 1571, 1589, and 1593 cm^{-1} (in the free ligand, not shown) that can be assigned to ring stretching modes of the pyridyl functions by comparison with the spectrum of 2-methylpyridine.[27] Except for the 1430 and 1475 cm^{-1} bands, these modes are of very low intensity in the mixed-valence complex (Figure 5b) but can be assigned to bands observed in the $Ru_2^{II,II}$ (1579 and 1603 cm^{-1}, Figure 5a) and $Ru_2^{III,III}$ state (1612 cm^{-1}, Figure 5c).

In the isovalent $Ru_2^{II,II}$ and $Ru_2^{III,III}$ forms (Figures 5a and 5c), strong bands observed at 1580 and 1536 cm^{-1}, respectively, can be assigned to the $\nu_{a(COO)}$ modes of the acetate ligands in

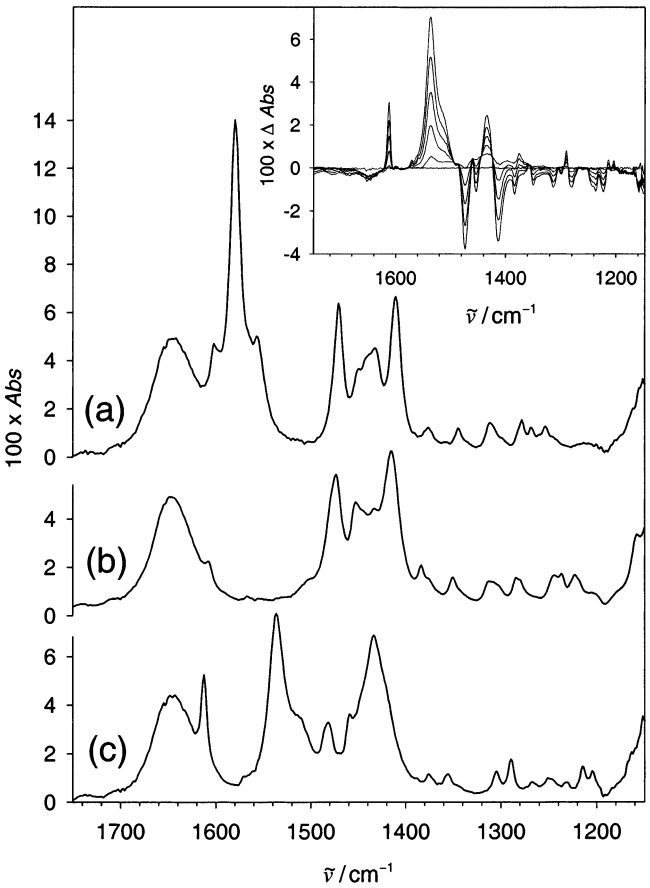

Figure 5. IR spectra of $[Ru_2(bpmp)(\mu\text{-}OAc)_2]^+$ (a), $[Ru_2(bpmp)(\mu\text{-}OAc)_2]^{2+}$ (b), and $[Ru_2(bpmp)(\mu\text{-}OAc)_2]^{3+}$ (c) in CD_3CN with 0.5 M $LiClO_4$. Spectra of $[Ru_2(bpmp)(\mu\text{-}OAc)_2]^+$ and $[Ru_2(bpmp)(\mu\text{-}OAc)_2]^+$ were observed spectroelectrochemically by electrolysis at 0.42 and −0.83 V. (Inset) Absorption changes upon oxidation at potentials between −0.03 and 0.42 V.

agreement with reported spectra for acetate-bridged $Ru_2^{II,II}$ (1582 cm^{-1})[28] and $Ru_2^{III,III}$ (1548 cm^{-1})[29] complexes. Similarly straightforward assignments based on the reported frequencies[28,29] can be made for the bands at 1410 cm^{-1} (Figure 5a, $Ru_2^{II,II}$), 1415 cm^{-1} (Figure 5b, $Ru_2^{II,III}$), and 1430 cm^{-1} (Figure 5c, $Ru_2^{III,III}$) that are attributed to the $\nu_{s(COO)}$ mode. In the case of the $Ru_2^{III,III}$ form (Figure 5c) the $\nu_{s(COO)}$ mode is superimposed onto the ring stretching mode of the pyridyl functions (see above) that is observed at 1430 cm^{-1} with the free ligand and the complex in all oxidation states.

For the mixed-valence state (Figure 5b) no band attributable to the $\nu_{a(COO)}$ mode is observed in the expected range of 1500−1600 cm^{-1}. Instead the band peaking at 1473 cm^{-1} appears to be a superposition of the $\nu_{a(COO)}$ mode and a pyridyl ring stretching mode that occurs at 1475 cm^{-1} in H-bpmp and the $Ru_2^{II,II}$ form of the complex (Figure 5a). The inset in Figure 5 shows the spectral changes upon gradual oxidation of $[Ru_2(bpmp)(\mu\text{-}OAc)_2]^{2+}$ at increasingly positive potentials where the bleaching at 1473 cm^{-1} and the concomitant rise at 1536 cm^{-1} are attributed to the $\nu_{a(COO)}$ mode of the $Ru_2^{II,III}$ and $Ru_2^{III,III}$ forms, respectively.

The IR spectra of the isovalent states are consistent with the $(\mu\text{-}OAc)_2$ formulation of the complex, while in the mixed valence state $\nu_{a(COO)}$ is not averaged[30] but is even more red-shifted than in the $Ru_2^{III,III}$ state, resulting in a remarkably small value of $\Delta\tilde{\nu} = 58$ cm^{-1} between $\nu_{a(COO)}$ and $\nu_{s(COO)}$. Such small $\Delta\tilde{\nu}$ is generally considered as an indication for an unusually short metal−metal distance or chelating coordination.[26] $\Delta\tilde{\nu} =$

36−70 cm^{-1} has been reported for $Ru_2^{II,III}$ complexes with a $Ru_2(\mu\text{-}O_2C\text{−}R)_4$ core that feature short Ru−Ru distances (∼2.3 Å) due to metal−metal bonds.[28] However, isovalent $Ru_2^{II,II}$ dimers with this bridging motif and the same short Ru−Ru distance show $\Delta\tilde{\nu} = 140\text{−}200$ cm^{-1}, i.e., typical values of bridging carboxylate ligands.[28,31]

Thus, the intriguingly small value of $\Delta\tilde{\nu}$ observed with $[Ru_2(bpmp)(\mu\text{-}OAc)_2]^{2+}$ seems to be a peculiarity of the mixed-valence state rather than a characteristic of the type of coordination or metal−metal distance. For cyano-bridged donor−acceptor complexes, red-shift of the cyanide stretching frequency has been reported and Endicott and co-workers have explained this effect in terms of vibronic coupling.[32,33] Generally, the curvature of the lower adiabatic potential energy curve is decreased and the force constant of a vibration coupled to electron transfer is lowered as an effect of vibronic coupling.[34] In the case of $[Ru_2(bpmp)(\mu\text{-}OAc)_2]^{2+}$, it is possibly the asymmetric acetate stretch coupled to electron-transfer that might explain the unexpected red-shift of the $\nu_{a(COO)}$ frequency and the small $\Delta\tilde{\nu} = 58$ cm^{-1} that are observed in the mixed-valence state only. The electronic spectrum indicates that electronic coupling is sufficiently strong to result in rapid electron tunneling, making the electron transfer rate essentially dependent on the frequency of coupled vibrational motions. Coupling of the electronic barrier crossing dynamics to the asymmetric stretch of the bridging acetate ligands would result in an electron transfer rate sufficiently fast to explain the narrow, solvent independent IT bands of $[Ru_2(bpmp)(\mu\text{-}OAc)_2]^{2+}$ (see above).

Conclusions

Much of the spectroscopic and electrochemical properties of $[Ru_2(bpmp)(\mu\text{-}OAc)_2]^{2+}$ can be rationalized in terms of both electronic delocalization (class III) and electronic localization in combination with rapid electron-transfer decoupled from solvent reorientation and a residual barrier to electron-transfer arising from inner reorganization (class II−III). Both assignments can account for the narrow, solvent independent IT bands, while the symmetric band shape and the results of the Hush analysis point to localization. Similar to the results of EPR spectroscopy, the magnitude of K_c and the absence of IC bands cannnot provide conclusive evidence for either assignment and the question of delocalization in $[Ru_2(bpmp)(\mu\text{-}OAc)_2]^{2+}$ remains open.

In a localized description, solvent averaging puts a lower limit of 4×10^{12} s^{-1} on the rate constant of electron transfer. Adiabatic electron transfer coupled to the asymmetric stretching mode of the acetate bridges would occur sufficiently fast and might explain the effect on the vibrational spectrum in terms of vibronic coupling.

Acknowledgment. The authors thank Leif Hammarström (Uppsala), Professor Björn Åkermark (Stockholm), and Professor Stenbjörn Styring (Lund) for continuous support. Financial support from the following organizations is gratefully acknowledged: The Knut and Alice Wallenberg Foundation, the Swedish Research Council, the Swedish National Energy Administration, and DESS.

References and Notes

(1) (a) *Mixed Valency Systems*: *Applications in Chemistry, Physics and Biology*; Prassides, K., Ed.; Kluwer Academic Publishers: Dordrecht, The Netherlands, 1991. (b) Raveau, B.; Michel, C.; Hervieu, M.; Provost, J.; Studer, F. In *Earlier and Recent Aspects of Superconductivity*; Bednorz, J. G., Müller, K. A., Eds.; Springer: New York, 1990; p 66.

(2) (a) Ward, M. D. *Chem. Soc. Rev.* **1995**, *24*, 121. (b) Launnay, J.-P. *Chem. Soc. Rev.* **2001**, *30*, 386. (c) *Mixed Valency Systems: Applications in Chemistry, Physics and Biology*; Prassides, K., Ed.; Kluwer Academic Publishers: Dordrecht, The Netherlands, 1991.

(3) Laidlaw, W. M.; Denning, R. G.; Verbiest, T.; Chauchard, E.; Persoons, A. *Nature*, **1993**, *363*, 58.

(4) (a) Nelsen, S. F. *Chem. Eur. J.* **2000**, *6*, 581. (b) Evans, C. E. B.; Naklicki, M. L.; Rezvani, A. R.; White, C. A.; Kondratiev, V. V.; Crutchley, R. J. *J. Am. Chem. Soc.* **1998**, *120*, 13096. (c) Demadis, K. D.; El-Samanody, E.-S.; Coia, G. M.; Meyer, T. J. *J. Am. Chem. Soc.* **1999**, *121*, 535. (d) Demadis, K. D.; Neyhart, G. A.; Kober, E. M.; White, P. S.; Meyer, T. J. *Inorg. Chem.* **1999**, *38*, 5948. (e) Ito, T.; Hamaguchi, T.; Nagino, H.; Yamaguchi, T.; Washington, J.; Kubiak, C. P. *Science* **1997**, *227*, 660. (f) Ito, T.; Hamaguchi, T.; Nagino, H.; Yamaguchi, T.; Kido, H.; Zavarine, I. S.; Richmond, T.; Washington, J.; Kubiak, C. P. *J. Am. Chem. Soc.* **1999**, *121*, 4625.

(5) For reviews see: (a) Allen, G. C.; Hush, N. S. *Prog. Inorg. Chem.* **1967**, *8*, 357. (b) Creutz, C. *Prog. Inorg. Chem.* **1983**, *30*, 1. (c) Sutin, N. *Prog. Inorg. Chem.* **1983**, *30*, 441. (d) Crutchley, R. J. *Adv. Inorg. Chem.* **1994**, *41*, 273. (e) Vance, F. W.; Williams, R. D.; Hupp, J. T. *Int. Rev. Phys. Chem.* **1998**, *17*, 307. (f) Chen, P.; Meyer, T. J. *Chem. Rev.* **1998**, *98*, 1439. (g) Brunschwig, B. S.; Sutin, N. *Coord. Chem. Rev.* **1999**, 187, 233. (h) Demadis, K. D.; Hartshorn, C. M.; Meyer, T. J. *Chem. Rev.* **2001**, *101*, 2655. (i) Brunschwig, B. S.; Creutz, C.; Sutin, N. *Chem. Soc. Rev.* **2002**, *31*, 168. (j) ref 2.

(6) Hush, N. S. *Prog. Inorg. Chem.* **1967**, *8*, 391.

(7) (a) Sutin, N. *Prog. Inorg. Chem.* **1983**, *30*, 441. Brunschwig, B. S.; Sutin, N. *Coord. Chem. Rev.* **1999**, *187*, 233. (b) Creutz, C.; Newton, M. D.; Sutin, N. J. *J. Photochem. Photobiol. A*: *Chem.* **1994**, *82*, 47.

(8) (a) Piepho, S. B.; Krausz, E. R.; Schatz, P. N. *J. Am. Chem. Soc.* **1978**, *100*, 2996. (b) Ondrechen, M. J.; Ko, J.; Zongh, L.-T. *J. Am. Chem. Soc.* **1987**, *109*, 1672. (c) Piepho, S. B. *J. Am. Chem. Soc.* **1988**, *110*, 6319.

(9) Robin, M. B.; Day, P. *Adv. Inorg. Chem. Radiochem.* **1967**, *10*, 247.

(10) Demadis, K. D.; El-Samanody, E.-S.; Coia, G. M.; Meyer, T. J. *J. Am. Chem. Soc.* **1999**, *121*, 535. Demadis, K. D.; Neyhart, G. A.; Kober, E. M.; White, P. S.; Meyer, T. J. *Inorg. Chem.* **1999**, *38*, 5948. Demadis, K. D.; Hartshorn, C. M.; Meyer, T. J. *Chem. Rev.* **2001**, *101*, 2655.

(11) The H-bpmp ligand has been widely used to synthesize dinuclear complexes of various transition metals, but no ruthenium complex with the H-bpmp ligand has been synthesized so far. (a) Borovik, A. S.; Papaefthymiou, V.; Taylor, L. F.; Anderson, O. P.; Que, L., Jr. *J. Am. Chem. Soc.* **1989**, *111*, 6183. (b) Berends, H. P.; Stephan, D. W. *Inorg. Chem.* **1987**, *26*, 749. (c) Diril, H.; Chang, H.-R.; Nilges, M. J.; Zhang, X.; Potenza, J. A.; Schugar, H. J.; Isied, S. S.; Hendrickson, D. N. *J. Am. Chem. Soc.* **1989**, *111*, 5102. (d) Suzuki, M.; Mikuriya, M.; Murata, S.; Uehara, A.; Oshio, H.; Kida, S.; Saito, K. *Bul. Chem. Soc. Jpn.* **1987**, *60*, 4305. (e) Seo, J. S.; Sung, N.-D.; Hynes, R. C.; Chin, J. *Inorg. Chem.* **1996**, *35*, 7472. (f) Torelli, S.; Belle, C.; Gautier-Luneau, I.; Pierre, J. L.; Saint-Aman, E.; Latour, J. M.; Le Pape, L.; Luneau, D. *Inorg. Chem.* **2000**, *39*, 3526. (g) Holman, T. R.; Wang, Z.; Hendrich, M. P.; Que, L., Jr. *Inorg. Chem.* **1995**, *34*, 134.

(12) For $Fe_2^{II,III}$ complexes with the H-bpmp ligand, the very weak intervalence band is most likely a superposition of several intervalence bands due to lower spin−orbit coupling of the first-row transition metal complexes. (a) Triest, M.; Davis, M. J.; Reber, C. *New J. Chem.* **1999**, *23*, 425. (b) Borovik, A. S.; Papaefthymiou, V.; Taylor, L. F.; Anderson, O. P.; Que, L., Jr. *J. Am. Chem. Soc.* **1989**, *111*, 6183.

(13) Diril, H.; Chang, H.-R.; Nilges, M. J.; Zhang, X.; Potenza, J. A.; Schugar, H. J.; Isied, S. S.; Hendrickson, D. N. *J. Am. Chem. Soc.* **1989**, *111*, 5102.

(14) For a dimer with nonnegligible delocalization, the net g tensor is the weighted sum $(1 - \alpha^2)g_a + \alpha^2 g_b$ of the contributions g_a and g_b from the metal sites M_a and M_b. If the principal axes of the single site g tensors are not collinear, g decreases with increasing α relative to a totally localized dimer. See, e.g., Westmoreland, T. D.; Wilcox, D. E.; Baldwin, M. J.; Mims, W. B.; Solomon, E. I. *J. Am. Chem. Soc.* **1989**, *111*, 6106.

(15) In the excited states the complex is more strongly delocalized but the EPR spectrum is arising from the ground-state only, although it leads to a description of all three doublets.

(16) See, e.g., (a) Bohan, T. L. *J. Magn. Res.* **1977**, *26*, 109. (b) McGarvey, B. R. *Coord. Chem. Rev.* **1998**, *170*, 75. (c) Solomon, E. I.; Hanson, M. A. in *Inorganic Electronic Structure and Spectroscopy*, Solomon, E. I., Lever, A. B. P., Eds.; Wiley: New York, 1999, Vol. II, p 57.

(17) Borovik, A. S.; Papaefthymiou, V.; Taylor, L. F.; Anderson, O. P.; Que, L., Jr. *J. Am. Chem. Soc.* **1989**, *111*, 6183.

(18) (a) Cotton, F. A.; Torralba, R. C. *Inorg. Chem.* **1991**, *30*, 2196. (b) Kasack, V.; Kaim, W.; Binder, H.; Jordanov, J.; Roth, E. *Inorg. Chem.* **1995**, *34*, 1924 and references therein.

(19) See, e.g., (a) Kaim, W.; Bruns, W.; Poppe, J.; Kasack, V. *J. Mol. Struct.* **1993**, *292*, 221. (b) Westmoreland, T. D.; Wilcox, D. E.; Baldwin, M. J.; Mims, W. B.; Solomon, E. I. *J. Am. Chem. Soc.* **1989**, *111*, 6106.

(20) Nelsen, S. F. *Chem. Eur. J.* **2000**, *6*, 581. Brunschwig, B. S.; Creutz, C.; Sutin, N. *Chem. Soc. Rev.* **2002**, *31*, 168.

(21) Brunschwig, B. S.; Creutz, C.; Sutin, N. *Chem. Soc. Rev.* **2002**, *31*, 168.

(22) The effective electron-transfer distance can be measured by Stark effect spectroscopy. See, e.g., Vance, F. W.; Williams, R. D.; Hupp, J. T. *Int. Rev. Phys. Chem.* **1998**, *17*, 307.

(23) See, e.g., (a) Neubold, P.; Wieghardt, K.; Nuber, B.; Weiss, J. *Inorg. Chem.* **1989**, *28*, 459. (b) Llobet, A.; Curry, M. E.; Evans, H. T.; Meyer, T. J. *Inorg. Chem.* **1989**, *28*, 3131. (c) Syamala, A.; Chakravarty, A. R. *Inorg. Chem.* **1991**, *30*, 4699. (d) Sasaki, Y.; Suzuki, M.; Nagasawa, A.; Tokiwa, A.; Ebihara, M.; Yamaguchi, T.; Kabuto, C.; Ochi, T.; Ito, T. *ibid.*, 4903. (e) Das, B. K.; Chakravarty, A. R. *Inorg. Chem.* **1991**, *30*, 4978.

(24) Horng, M. L.; Gardecki, J. A.; Papazyan, A.; Maroncelli, M. *J. Phys. Chem.* **1995**, *99*, 17311.

(25) Richardson, D. E. In *Inorganic Electronic Structure and Spectroscopy*, Solomon, E. I., Lever, A. B. P., Eds.; Wiley: New York, 1999, Vol. II, pp 146−170.

(26) (a) Deacon, G. B.; Phillips, R. J. *Coord. Chem. Rev.* **1980**, *33*, 227. (b) Nakamoto, K. *Infrared and Raman Spectra of Inorganic and Coordination Compounds*, Wiley: New York, 1997; Part B, pp 59−62. (c) Nara, M.; Torii, H.; Tasumi, M. *J. Phys. Chem.* **1996**, *100*, 19812.

(27) Green, J. H. S.; Kynaston, W.; Paisley, H. M. *Spectrochim. Acta* **1963**, *19*, 549.

(28) Lindsay, A. J.; Wilkinson, G.; Motevalli, M.; Hursthouse, M. B. *J. Chem. Soc., Dalton Trans.* **1987**, 2723.

(29) Neubold, P.; Wieghardt, K.; Nuber, B.; Weiss, J. *Inorg. Chem.* **1989**, *28*, 459.

(30) For class III systems coalescence of ligand vibration frequencies is observed. See, e.g., DeRosa, M. C.; White, C. A.; Evans, C. E. B.; Crutchley, R. J. J. *Am. Chem. Soc.* **2001**, *123*, 1396 and references therein.

(31) Aquino, M. A. S. *Coord. Chem. Rev.* **1998**, *170*, 141.

(32) Bignozzi, C. A.; Argazzi, R.; Schoonover, J. R.; Gordon, K. C.; Dyer, R. B.; Scandola, F. *Inorg. Chem.* **1992**, *31*, 5260.

(33) (a) Watzky, M. A.; Endicott, J. F.; Song, X.; Lei, Y.; Macatangay, A. *Inorg. Chem.* **1996**, *35*, 3463. (b) Watzky, M. A.; Macatangay, A. V.; Van Camp, R. A.; Mazzetto, S. E.; Song, X.; Endicott, J. F.; Buranda, T. *J. Phys. Chem. A* **1997**, *101*, 8441. (c) Endicott, J. F.; Watzky, M. A.; Song, X.; Buranda, T. *Coord. Chem. Rev.* **1997**, *159*, 295. (d) Macatangay, A. V.; Mazzetto, S. E.; Endicott, J. F. *Inorg. Chem.* **1999**, *38*, 5091.

(34) See, e.g., Grochala, W.; Hoffmann, R. *J. Phys. Chem. A* **2000**, *104*, 9740 and references therein.